Supporting Information

Water-resilient carbon nanotube based strain sensor for monitoring structural integrity

Preety Ahuja[1], Shingo Akiyama[1], Sanjeev Kumar Ujjain[1], Radovan Kukobat[1], Fernando Vallejos-Burgos[1], Ryusuke Futamura[1], Takuya Hayashi[2], Mutsumi Kimura[3], David Tomanek[4], Katsumi Kaneko[1,*]

[1]Research Initiative for Supra-Materials, Shinshu University, Nagano, Japan

[2]Department of Water Environment and Civil Engineering, Faculty of Engineering, Shinshu University, Nagano, Japan

[3]Faculty of Textile Science and Technology, Shinshu University, Ueda, Japan

[4]Physics and Astronomy Department, Michigan State University, East Lansing, Michigan 48824, USA

Corresponding Author

*E-mail ID: kkaneko@shinshu-u.ac.jp

Contents

Figure S11. SEM micrographs of embedded sensor (PDMS/SWCNT/PDMS) before (a,b) and after 15k loading-unloading cycling (c,d).

Figure S12. Real time response of the sensor in electrical circuit connected to LED (a), under applied strain (b-d). Loading of strain decreases the illumination intensity of LED whereas unloading of strain follows the opposite trend.

Table S1. Tabulated data to compare the performance of other CNT based stretchable strain sensor.

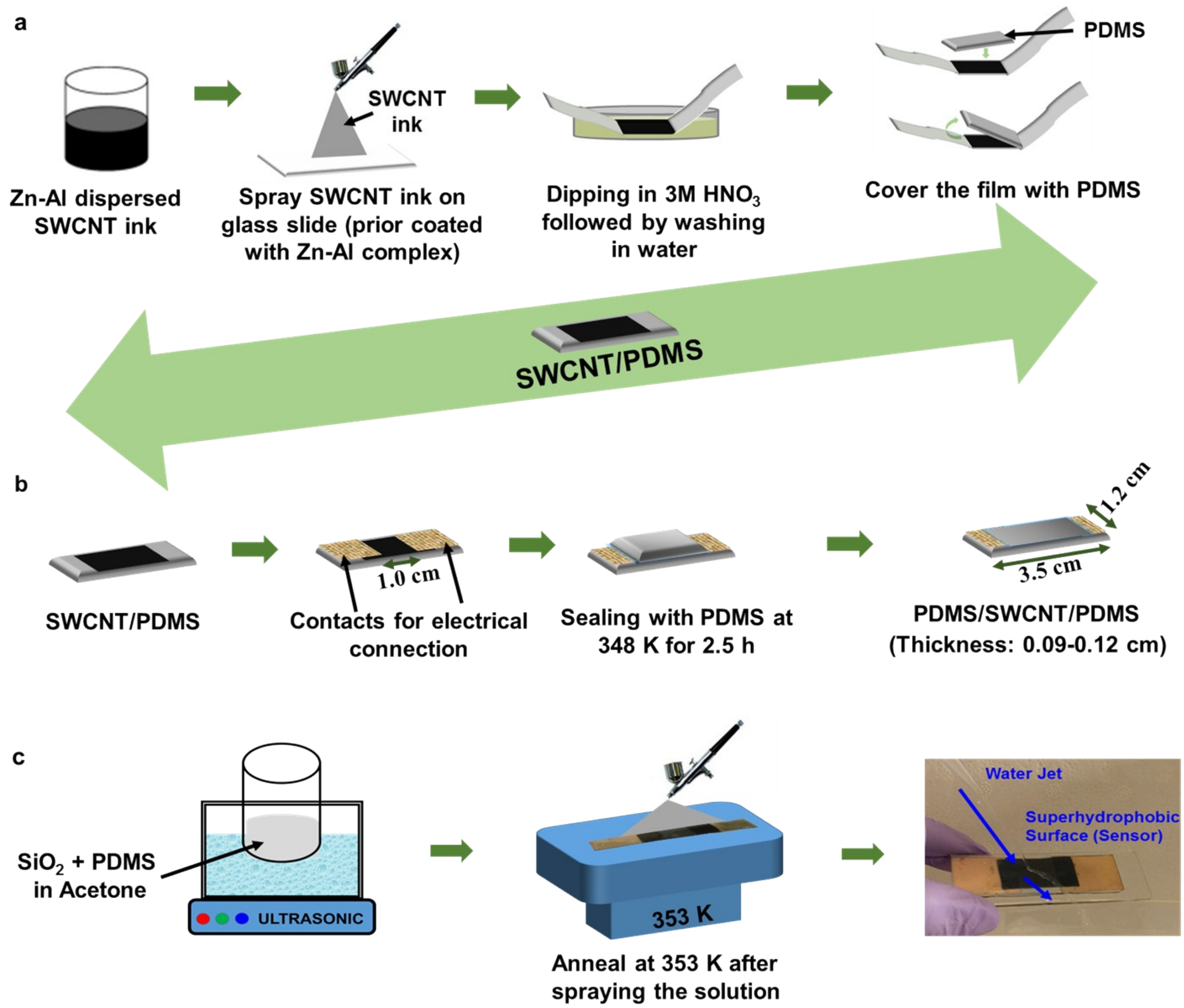

Figure S1. (a) SWCNT film formation process and transfer of film onto PDMS (SWCNT/PDMS), (b) Fabrication of embedded sensor, (PDMS/SWCNT/PDMS) and (c) Encapsulation of the fabricated sensor in water repellant coating (blue arrow shows the direction of water jet).

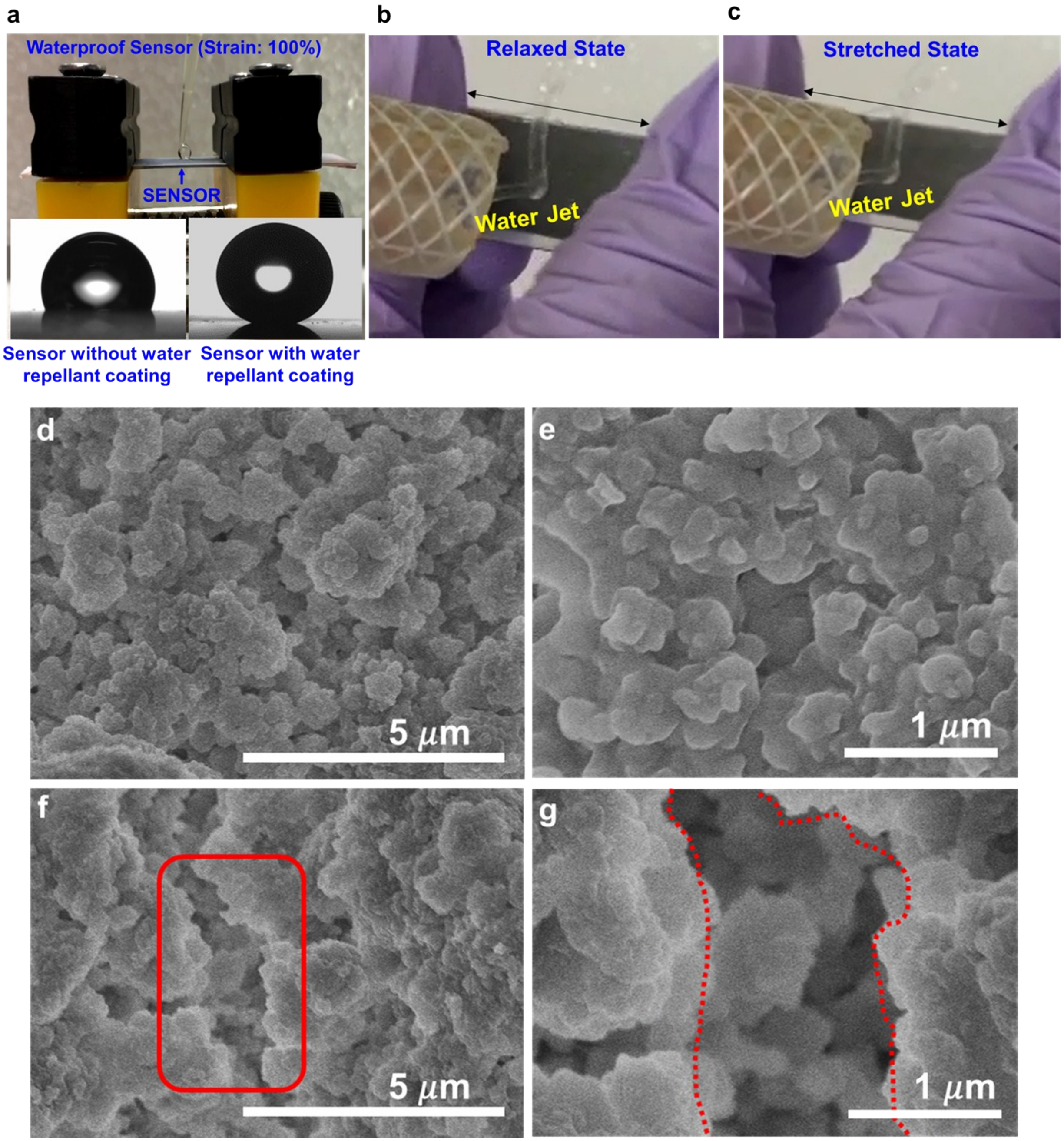

Figure S2. (a) Photographic image of waterproof sensor at 100% strain, inset shows water droplet on the surface of sensor with and without water repellant coating, Photographic image of water jet blocking at relaxed (b) and strained surface (c) of waterproof sensor, SEM micrographs of sensor under unstrained (d and e) and strained (f and g) states.

SEM micrographs of the superhydrophobic surface of sensor shows dual scale morphology, where nanoscale pseudo-spherical particles of SiO_2 aggregate to form microscale clusters. These clusters having dual scale roughness are covered with layer of PDMS, which not only decrease its surface energy but also maintain their structural integrity, making them stable superhydrophobic. Under unstrained state (Figure S2 d & e), a uniform layer of these clusters can be seen, while cracks formation on top surface can be revealed from Figure S2 f & g for sensor under strained state. Noteworthy, the water resiliency of the sensor remains invariable, as the sensor possesses similar morphology even under the cracks. This reflects the stability of the present water resilient sensor under unstrained and strained states.

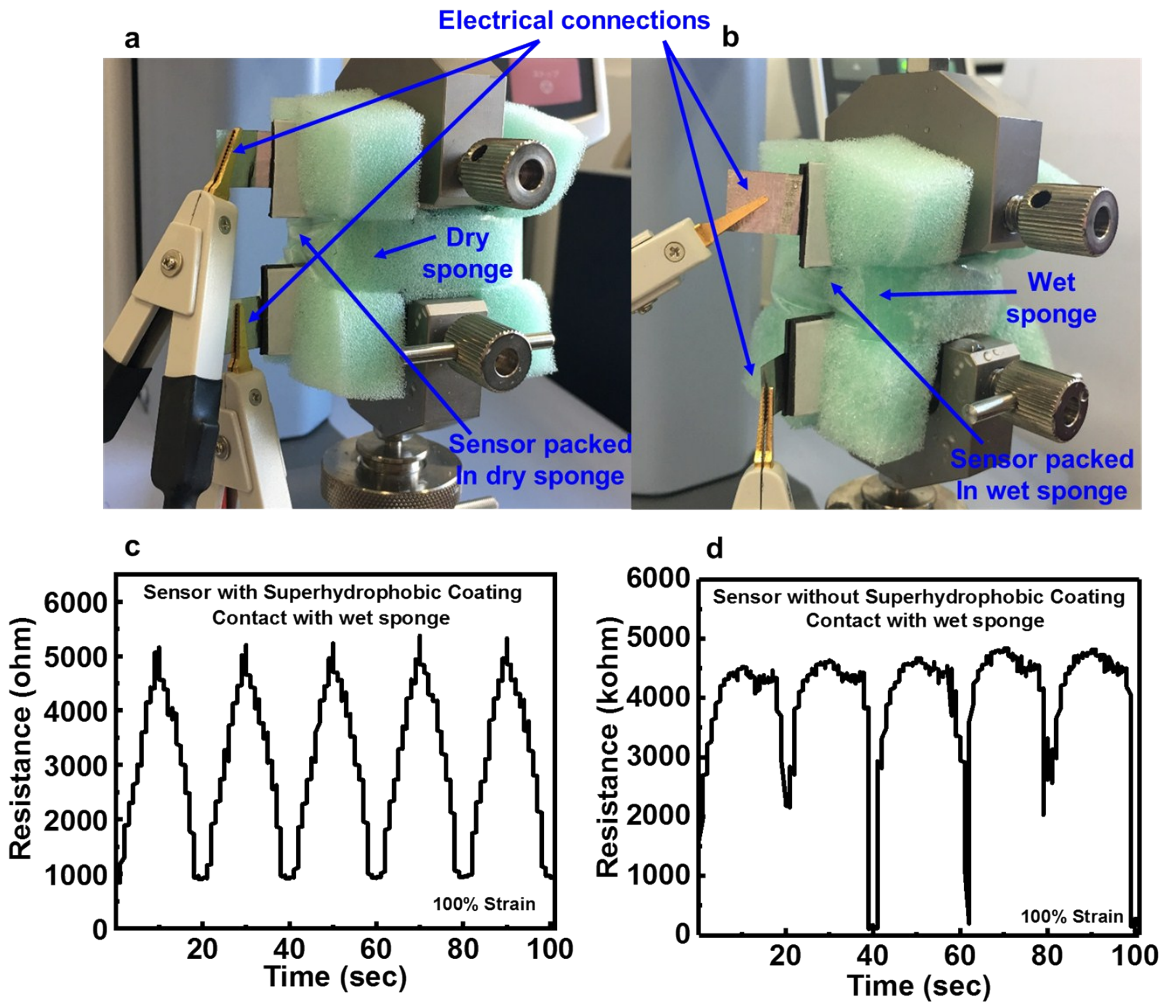

Figure S3 Image of the water proof sensor packed in sponge under dry (a) and wet (b) conditions, Actual response of the sensor in contact with wet sponge (c) with and (d) without superhydrophobic coating.

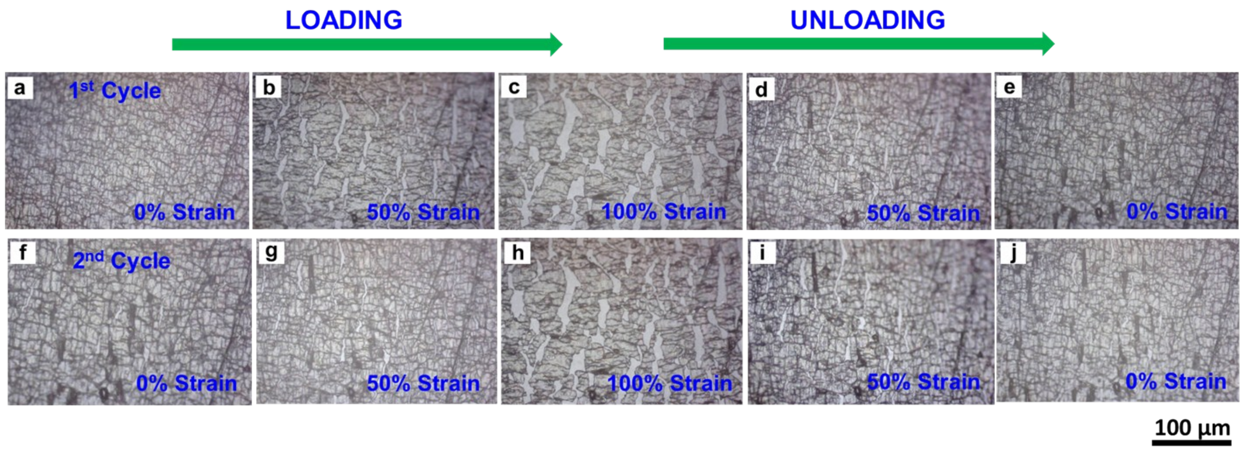

Figure S4. Optical Micrographs of SWCNT@PDMS during first (a-e) and second (f-j) loading-unloading (0% →100%→0%) cycle.

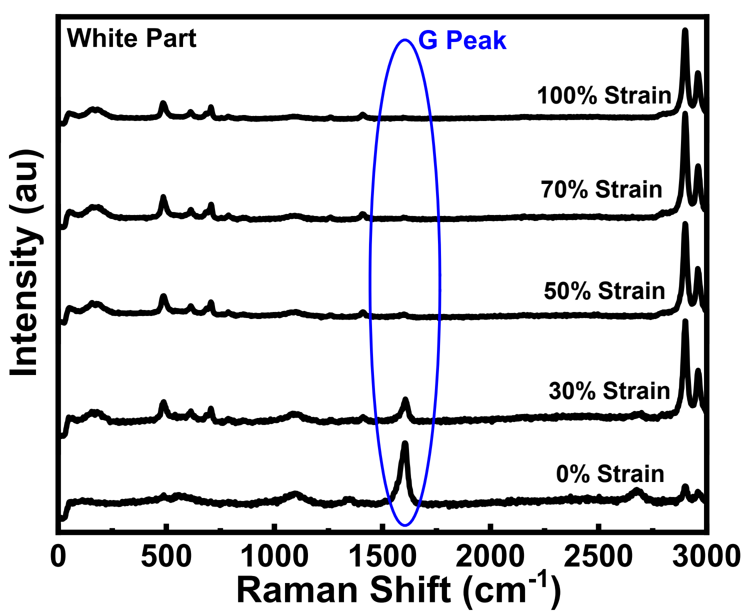

Figure S5. In situ Raman Spectra of the SWCNT@PDMS (white part) at particular strains during initial strain cycle (0→100%).

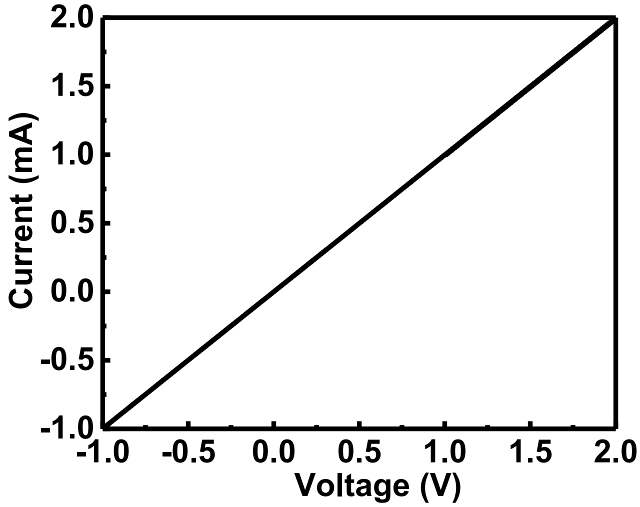

Figure S6. Current (I) - Voltage (V) Characteristics of Embedded Strain Sensor (PDMS/SWCNT/PDMS).

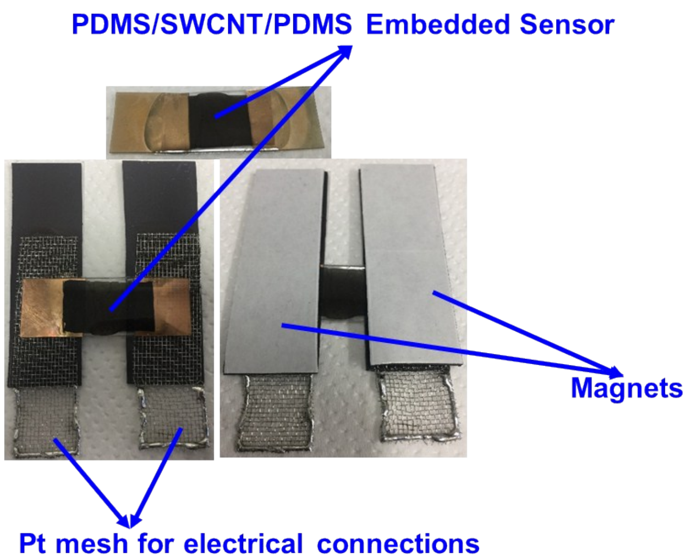

Figure S7. Electrical connections of the fabricated sensor with Pt mesh in between magnets.

The sensor was firmly fixed between Pt mesh to keep stable electrical contact with 1 cm^2 as an effective sensor area for stretching. In order to avoid the mismatch between actual strain and actuator displacement, we use Pt mesh as it provides the rigid holding to PDMS.

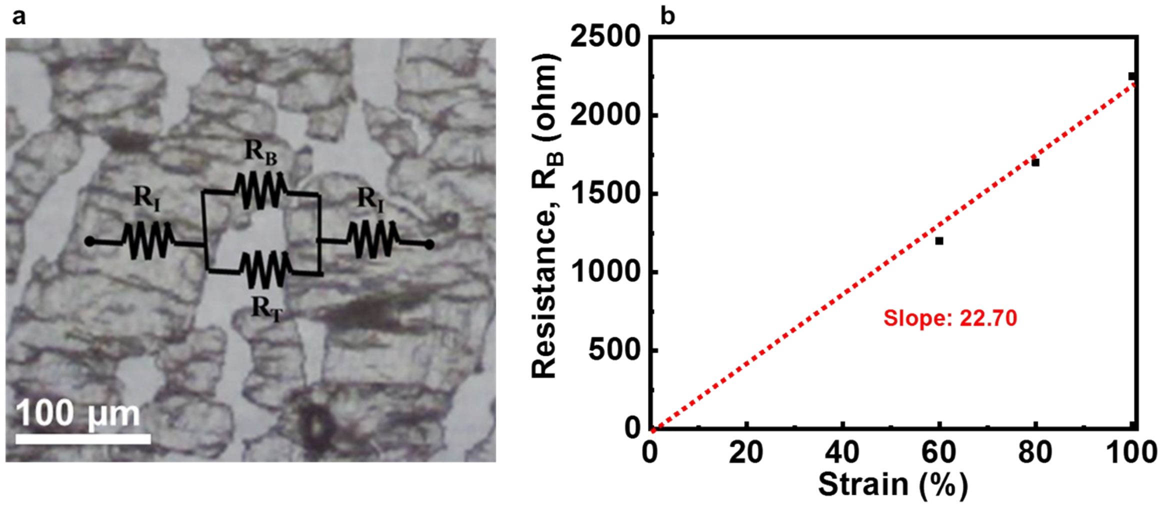

Figure S8. Resistance model (a) to describe the mechanism in resonse to applied strain and (b) Linear variation of R_B, bridge resistance with applied strain (higher strain).

Initial resistance reflects the inter SWCNT-SWCNT contact resistance in PDMS film. Further, the formation of cracks at higher strain induces R_B, bridge resistance and R_V, tunneling resistance.

For simplicity, we neglect the capacitive contribution at higher strains.

$$R = \frac{2R_I R_B + 2R_I R_V + R_B R_V}{R_B + R_V}$$

At higher Strains, $R_v >>> R_I, R_B$

$$R = \frac{2\frac{R_I R_B}{R_V} + 2R_I + R_B}{\frac{R_B}{R_V} + 1}$$

$$R = 2R_I + R_B$$

R_B is calculated at higher strains (60, 80 and 100% strain) and it should be zero at 0% strain.

Hence, Linear fit to R_B vs Strain ($\mathcal{E}$) satisfies the linear relationship, $R_B = 22.7 \text{ X } \mathcal{E}$.

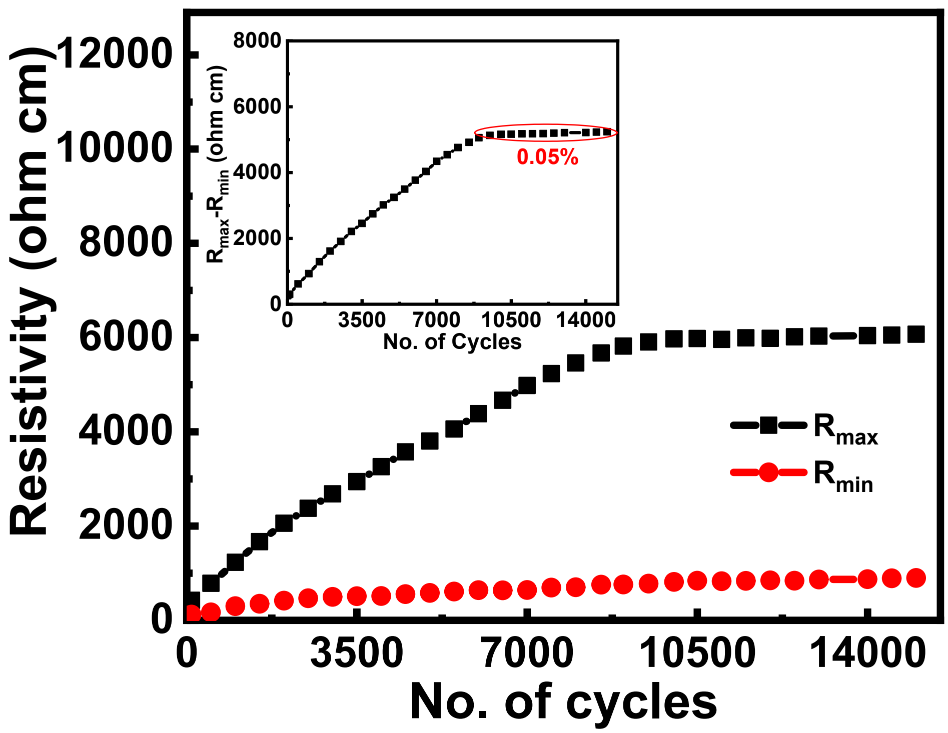

Figure S9. Change in resistivity of the sensor during 15k loading-unloading cycles.

R_{max} and R_{min} of the multiple cycles demonstrates slight changes during continual stretching under large strain of 100 %. This is precisely displayed by the difference in R_{max} and R_{min} in inset which clearly shows increment in resistance change owing to stabilization process till 7000 cyles followed by the steady performance.

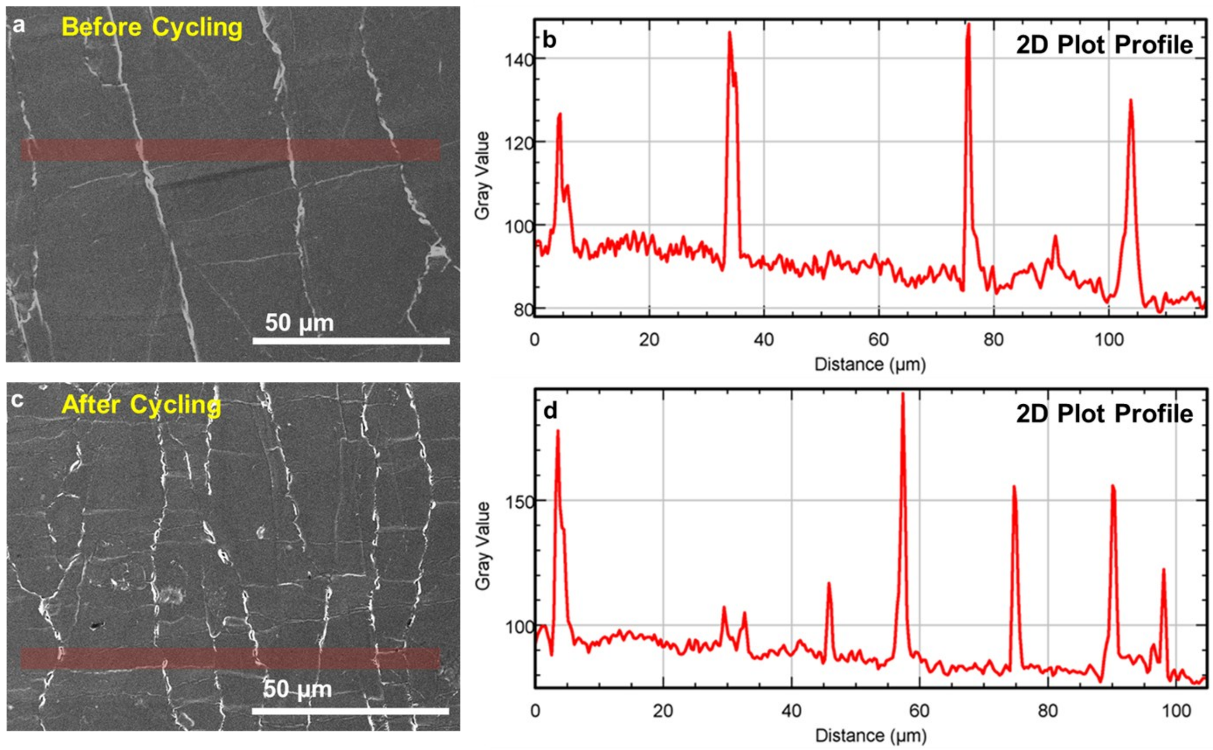

Figure S10. Analysis of SEM micrograph for 2D Profile by Image J software of the sensor, before (a,b) and after 15k cycling (c,d).

The creased SWCNT film on PDMS substrate was imaged by SEM and found to have crease density of ~400 per mm^2 (a). A 2D profile was also generated using Image J software (b) showing the gray value of the creases. The continuous cycling of the sensor to 100% strain increases the crease density (c and d), offering stable and reliable response.

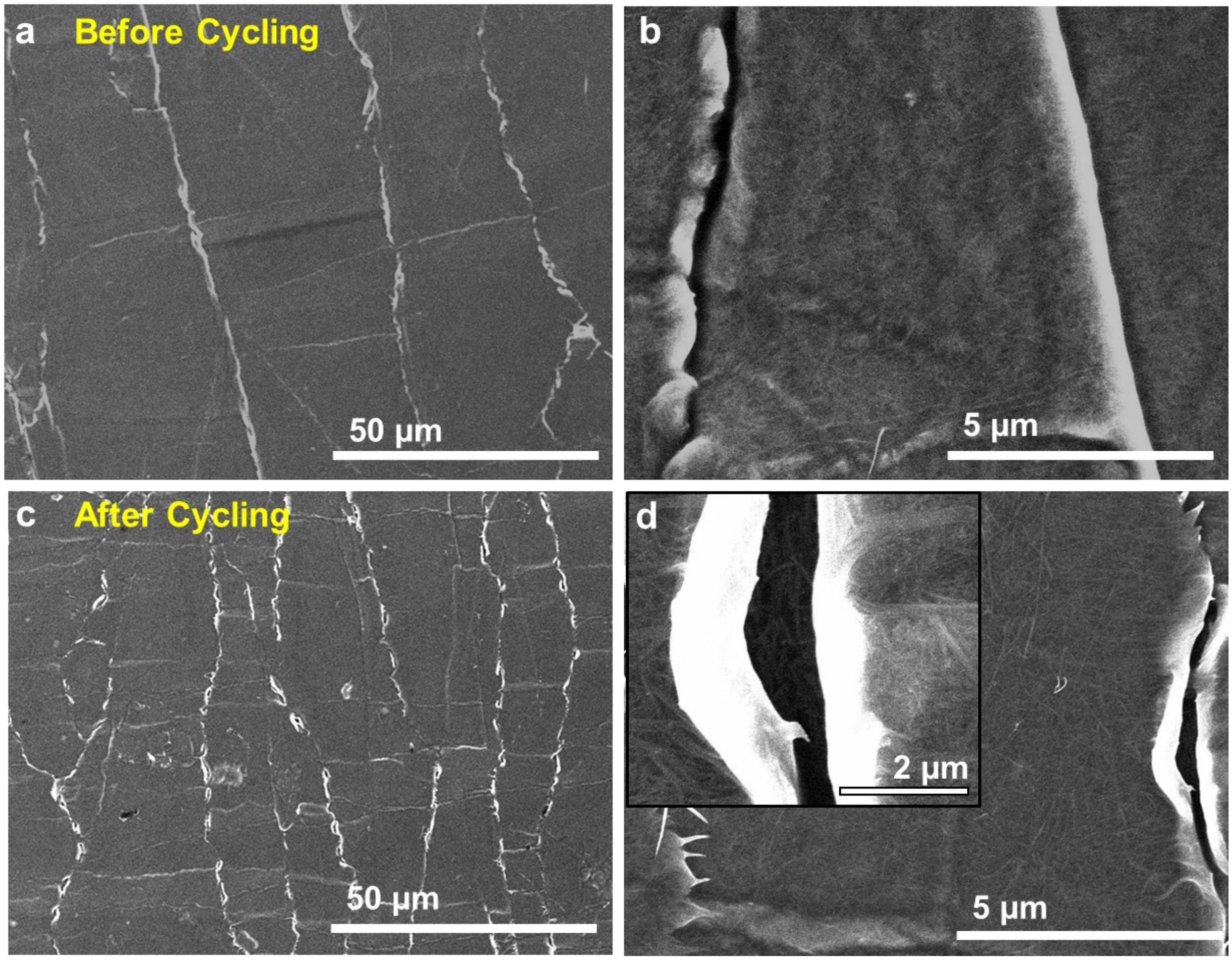

Figure S11. SEM micrographs of embedded sensor (PDMS/SWCNT/PDMS) before (a,b) and after 15k loading-unloading cycling (c,d).

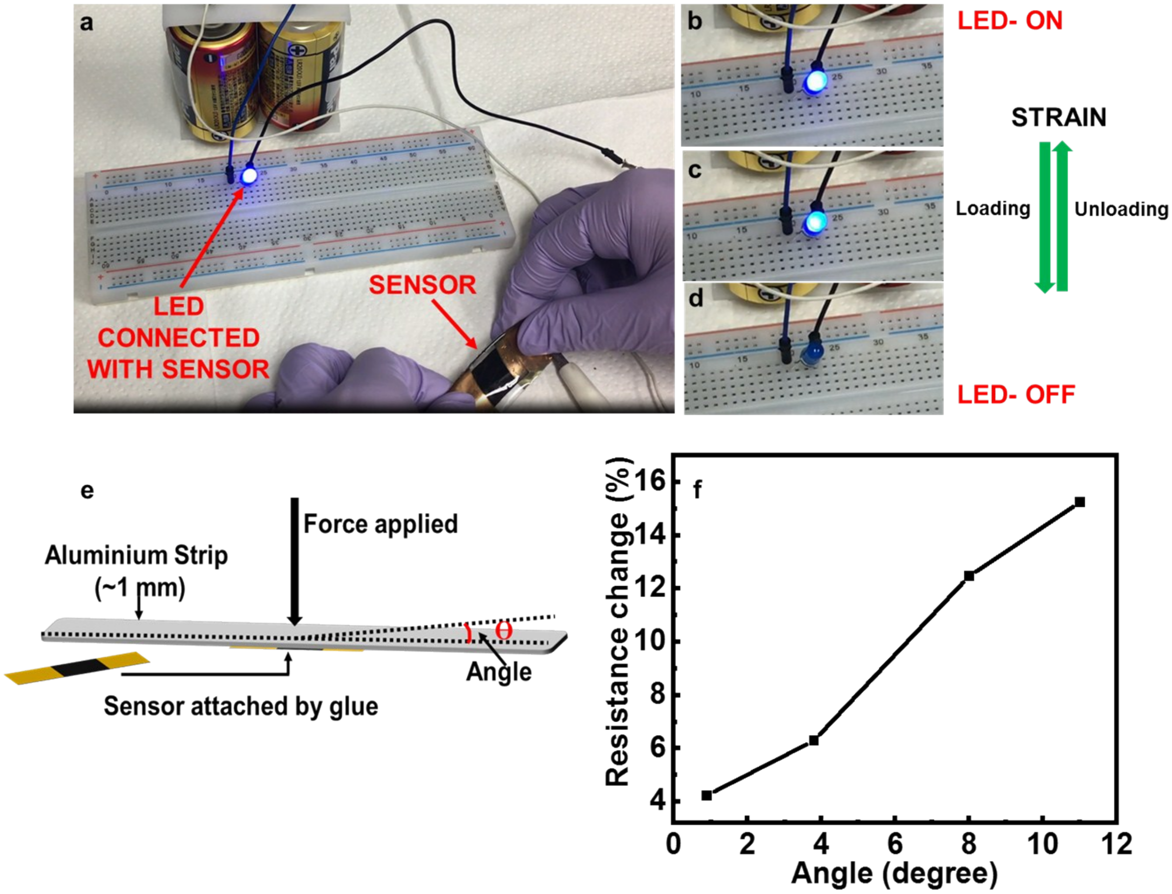

Figure S12. Real time response of the sensor in electrical circuit connected to LED (a), under applied strain (b-d). Loading of strain decreases the illumination intensity of LED whereas unloading of strain follows the opposite trend. (e) Schematic showing attachment of sensor to aluminium strip and (f) Resistance change with applied strain (change in angle) to monitor the structural integrity of aluminium strip.

1. **Supplementary Table**

S. No.	SENSOR	Stretchability+ Cycling Stability	Linear Response + Gauge Factor	Waterproof Properties	References
1	Cracked SWCNT film embedded in PDMS	50%	0-10% 10-50% G.F. 2 X 10^6 at ϵ<5% 10^7 at ϵ=50%	—	26
2	Thickness gradient film by self-pinning effect Carboxylic acid modified SWCNT on PDMS	140%	3 linear regions G.F. 161 @ 0< ϵ<2% 9.8 @ 2< ϵ<15% 0.58 @ ϵ>15%	—	27
3	MWCNT in PDMS	40%	2 linear regions (GF -) 0< ϵ<10% 10%< ϵ<40%	—	9
4	SACNT/PDMS composite Superaligned CNT by CVD	400%	R_o= 22.7 kohm G.F. 0.12 (0-100%) 0.075 (100-300%) 0.2 (300-400%)	—	45
5.	Paraffin wax-polyolefin thermoplastic blend with carbon nanofibers	700%	—	In-situ Contact Angle 150^o	6
6.	SWCNT/Ag NP with fluoropolymer coated PDMS	4% or less	Linear G.F.--	Water and Saline water resistant	4
7.	MWCNT with Fe_3O_4 in TPE	76%	G.F. 15.6 ϵ<6% 8.1 15-50% 5.4 55-76%	ϵ=0 160^o ϵ=25 156^o ϵ=50 151^o Acid & Alkali Resistant ~157^o-160^o	7
8.	Creased SWCNT embedded in PDMS	100%	Highly linear response G.F. ~5	Water, Alkaline, acidic and Saline water resistant ϵ=0 162°±0.4 ϵ=100 161°±0.8	**Our Work**

Table S1. Tabulated data to compare the performance of other CNT based stretchable strain sensor.